N72-23790

CORRELATION OF APOLLO OXYGEN TANK THERMODYNAMIC PERFORMANCE PREDICTIONS

H. W. Patterson
The Boeing Company
Space Division
Houston, Texas

ABSTRACT

Parameters necessary to analyze the stratified performance of the Apollo oxygen tanks include "g" levels, tank elasticity, flow rates and pressurized volumes. Methods for estimating "g" levels and flow rates from flight plans prior to flight, and from guidance and system data for use in the post flight analysis are described. Equilibrium thermodynamic equations are developed for the effects of tank elasticity and pressurized volumes on the tank pressure response and their relative magnitudes are discussed. Correlations of tank pressures and heater temperatures from flight data with the results of the stratification model developed by C. K. Forester are shown. Heater temperatures were also estimated with empirical heat transfer equations. Empirical equations were found to yield satisfactory agreement with flight data when fluid properties were averaged rather than evaluated at the mean film temperature.

NOMENCLATURE

Symbols

A	Area
b	Tank wall thickness
C_k	Constant in heater temperature sensor lag equation
C_p	Specific heat at constant pressure
C_s	Stefan Boltzman constant
C_{ra}	Constant in Rayleigh number heat transfer equation
D	Diameter
E	Young's modulus

Symbols

$\overline{F}$	Thrust vector
$\overline{g}$	Acceleration in Earth gravity units
GM	Product of gravitational constant and attracting body mass
h	Enthalpy
I	Vehicle inertia matrix
K	Thermal conductivity
L	Length
M	Mass
MC	Heater thermal mass
N	Polytropic exponent
P	Pressure
Q	Quantity of heat
$\overline{R}$	Position vector
R_a	Rayleigh number
r	Tank radius
T	Temperature
t	Time
U	Internal energy
V	Volume
$\overline{\alpha}$	Vehicle angular acceleration vector
β	Coefficient of thermal expansion
ε	Heater emissivity (0.2 assumed)
ρ	Density
ϕ	Thermodynamic property, $\frac{1}{\rho\frac{\partial U}{\partial P}}$
θ	Thermodynamic property, $-\rho\frac{\partial h}{\partial \rho}$
σ	Poisson's ratio
μ	Viscosity
$\overline{\omega}$	Vehicle angular velocity vector

Subscripts

b	Bulk fluid
cg	Center of gravity
d	Demand
f	Thrust
g	Attracting body (earth or moon)
h	Heater
L	Lines
o	Reference state or condition
t	Tank
s	Sensor

INTRODUCTION AND SUMMARY

Flight performance of single phase cryogenic tanks (pressure decays and heater temperatures) can be reasonably predicted by the techniques developed for the Apollo oxygen tanks. Very careful attention is necessary in the determination of flight operating conditions (accelerations and flow rates) to obtain accurate flight predictions.

The primary analysis tool used for the tank thermodynamic predictions was the numerical model* developed by C. K. Forester for a non-isothermal cryogen. It was evident that if this analysis method were to provide accurate flight predictions:

1. Acceleration must be accurately established to model the convection processes in the tank, and

2. Accurate flow rates are required to determine the pressure response to heat addition.

Procedures to calculate these accelerations and flow rates for Apollo 14 were developed. Early comparisons of the simulation results to flight data indicated that additional effects, such as heater thermal mass and tank elasticity, needed to be included in the basic solution. The basic method of solution did not require modifications. The resulting prediction techniques have been correlated to Apollo 14 flight data and show excellent agreement.

*Forester, C. K., "Pressurized Expulsion of Non-Isothermal Single Phase Cryogen", paper presented at the NASA-MSC Cryogenics Symposium, May 20-21, 1971.

Heater temperatures analyses were also made with an empirical Rayleigh number equation for convection. The fluid properties for this simplified analysis were averaged instead of evaluated using standard conventions. This approach resulted in good correlations with flight data and provides a convenient tool for heater temperature predictions.

SYSTEM DESCRIPTION

The oxygen flow distribution system is shown by Figure 1. The system includes check valves which are intended to prevent flow into the tanks during normal operation. The isolation valve between tanks 2 and 3 is normally open and for the Apollo 14 mission was closed only during the high flow test. The flow restrictors are capillary tubes which produce a pressure drop of approximately 800 psi at 3.5 lbs/hr flow rate. The restrictors are the only significant source of pressure drop in the system.

The data available from the system include fluid quantity and pressure, and heater temperature for each of the three cryogenic tanks. The surge tank is instrumented to provide pressure data only. The flow rate to the environmental control system is measured downstream of the surge tank and, therefore, includes contributions from all four of the tanks. The flow rate to the fuel cells is also measured, but can be more accurately determined from the electrical current.

FLOW RATES

The total flow from the three tanks during the Apollo 14 mission was determined from the fuel cell usage and the flow rate across the restrictors to the environmental control system (ECS). The fuel cell flow rate was computed using the fuel cell current, because the current data are more accurate than the fuel cell flow meters. The flow rate across the restrictors during high flow periods was based on the restrictor pressure drop calibrations. During low flow periods, the restrictor flows were obtained from the ECS flow rate (measured downstream of the restrictors) and the net change of mass in the surge tank during the period.

The flow rates from the individual cryogenic tanks were not measured, therefore, it was necessary to divide the total system flow among the three tanks. The individual tank flow rates were determined from the total system flow on the basis of equilibrium tank thermodynamics. The pressure differences between tanks were used to determine the check valves configuration and to constrain the thermodynamics calculations.

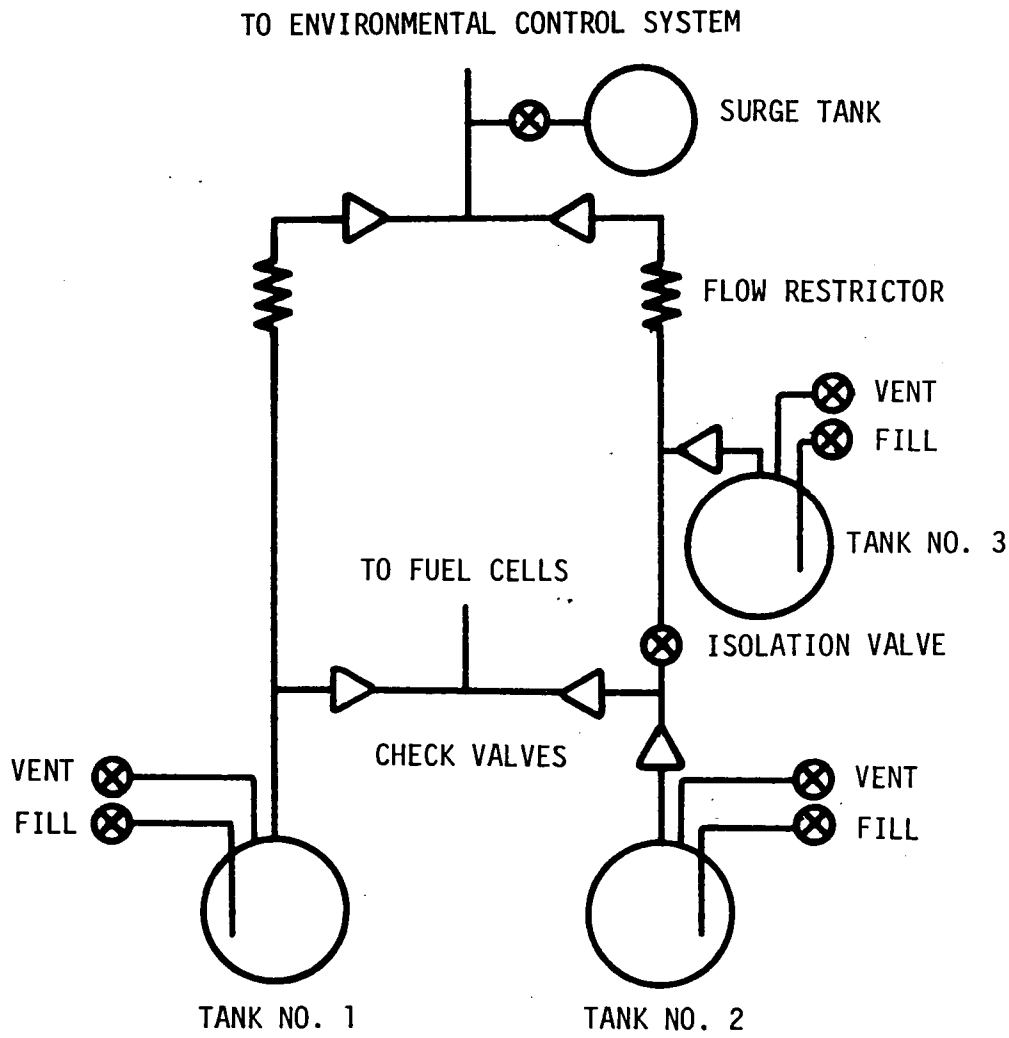

FIGURE 1 - APOLLO 14 OXYGEN SYSTEM FLOW SCHEMATIC

The flow distribution is affected by the heat input to the separate tanks, therefore, the heat leaks were estimated from flight data. The tank 1 and tank 3 heat leaks were found to be nominal at zero flow rate at 90% and 10% quantities, respectively. The tank 2 heat leak was not verified, but is believed to have been slightly greater than nominally expected. The tank 2 heat leak could not be determined for a zero flow condition because the check valve provided to isolate the tank leaked. The check valve permitted warm fluid to flow back into the tank causing warming of the insulation and increasing the heat leak.

The flow rate distributions were obtained by simultaneous solution of the pressure change equations (Appendix) for the tanks supplying the system flow. The calculations included the effects of tank elasticity, since the elasticity strongly affects the pressure change rate at high quantities (Figure 2). The simultaneous solution of equations A-19 for two tanks supplying the system demand relates the individual tank flow to the total flow. The total flow used for this calculation included the flow rate required to pressurize the external line volumes. These calculations are simplified if the pressure change rate is known and used with the nominal heat leak to determine the individual tank flows. The flow rates from this method are in the same ratio as those provided by simultaneous solution of the equations.

The tank 2 check valve leak required special consideration to determine the flow into the tank causing pressurization. The flow rate into the tank was determined from the volume change required to produce the observed pressure change. Using equation A-15 and considering the volume change due to a hot bubble as well as tank elasticity, the pressure change is:

$$\frac{dP}{dt} = \frac{\phi}{V}\left(\frac{dQ}{dt} + \theta\,\frac{dM_d}{dt}\right) - \frac{1}{V}\,\rho_t\theta\phi\left[\left(\frac{dV}{dt}\right)_t + \left(\frac{dV}{dt}\right)_L\right] \qquad (1)$$

where $\left(\frac{dV}{dt}\right)_L$ is the volume change due to a bubble of fluid at the line density.

During pressurization, the demand flow $\frac{dM_d}{dt}$ is zero. Substituting $-\frac{1}{\rho_L}\frac{dM}{dt}$ for $\left(\frac{dV}{dt}\right)_L$ and solving for $\frac{dM}{dt}$ we have:

$$\frac{dM}{dt} = \frac{\rho_L}{\rho_t}\,\frac{V}{\phi\theta}\left[\frac{dP}{dt} - \frac{\phi}{V}\,\frac{dQ}{dt} + \frac{1}{V}\,\rho_t\phi\theta\left(\frac{dV}{dt}\right)_t\right] \qquad (2)$$

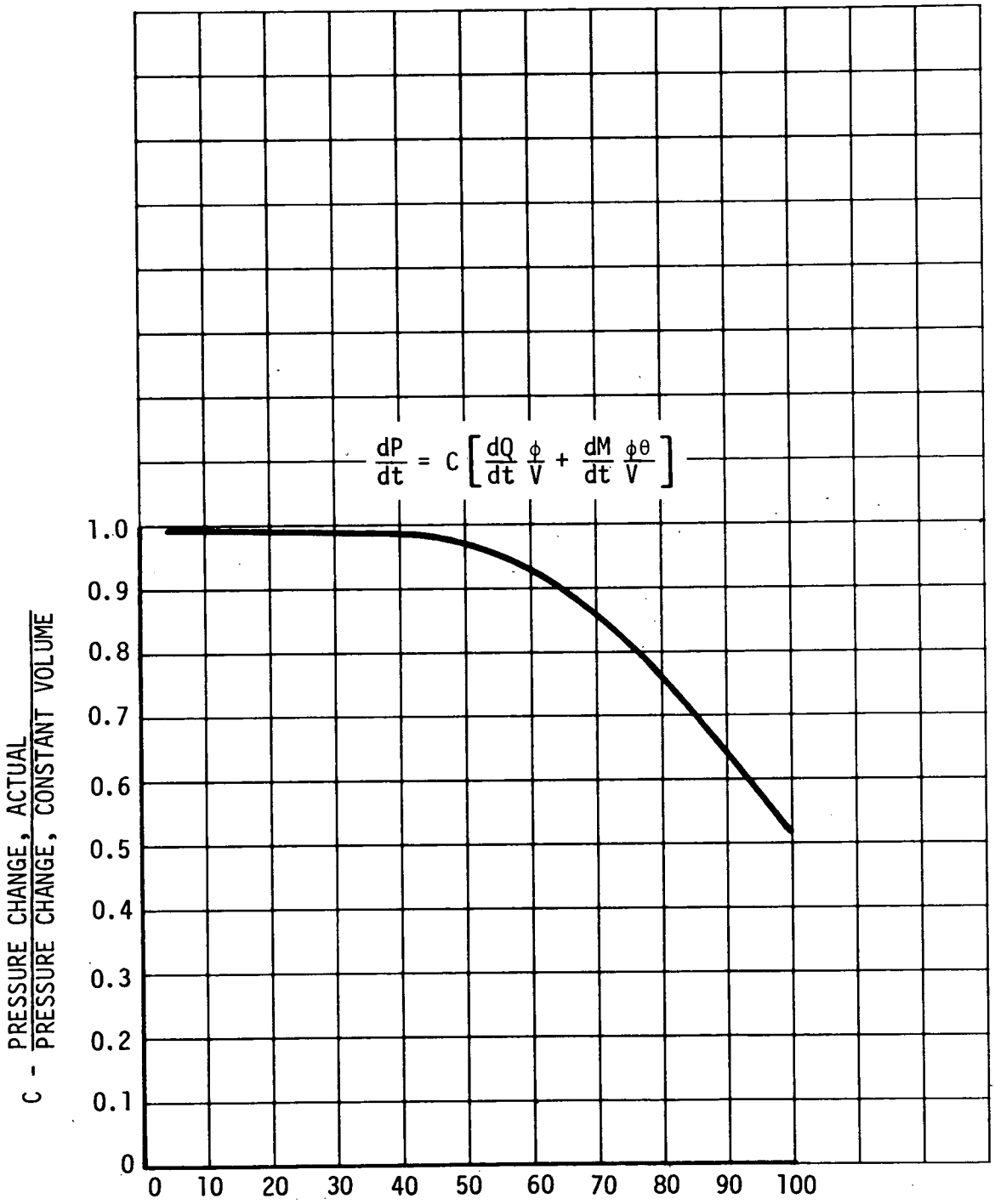

FIGURE 2 - OXYGEN TANK ELASTICITY EFFECT

This method of determining tank 2 inflow during the tank 3 heater cycle at 26 hours AET resulted in check valve leakage rates of approximately 0.05 lbs/hr which is believed to be realistic.

Thermodynamic analyses were not required to distribute the flows during the high flow test, since the isolation valve was closed. The tank 3 flow rates (Figure 3) during the tests were determined from the restrictor pressure drop while the surge tank valve was open. Flow rates were assumed constant while the surge tank valve was closed. The tank 1 flow rates (Figure 4) were also determined from the restrictor pressure drop, but included the fuel cell flow rate when the tank 1 pressure was greater than the tank 2 pressure.

TANK ACCELERATION ANALYSIS

The sources of accelerations in a space vehicle in drifting flight include vehicle rotations, thrusts caused by fluid venting, gravity gradients and solar pressure. The solar pressure is approximately 10^{-7} lbs/ft^2 and produces an acceleration of less than 5×10^{-9} "g" for the Apollo vehicle. The acceleration due to solar pressure was an order of magnitude smaller than the accelerations produced by vehicle rotations during a typical Apollo 12 attitude hold period and was, therefore, neglected.

The procedure for the analysis of accelerations during attitude hold conditions used rotation rates from guidance data directly for the centripetal acceleration. The rotation rates were numerically differentiated for the angular acceleration term. The total acceleration due to rotation is:

$$32.174\ \bar{g} = \bar{\omega} \times \bar{\omega} \times (\bar{R}_t - \bar{R}_{cg}) + \bar{\alpha} \times (\bar{R}_t - \bar{R}_{cg}) \qquad (3)$$

Telemetry data from the digital auto pilot used for the analysis includes the three components of the $\bar{\omega}$ vector and the calculation is, in principle, straightforward. Some difficulty does, however, arise due to the angular acceleration. The angular acceleration terms tends to dominate the centripetal term because the centripetal acceleration depends on the square of the rotation rate. The acceleration term also introduces questions of significance due to the short durations of application. Typically, the reaction control system jet firings cause angular accelerations greater than 2×10^{-4} radians/second^2, but the duration is of the order of 10 milliseconds. This acceleration results in a movement of the oxygen tank of about 10^{-7} inches during the time the acceleration is applied. This small displacement would appear to be negligible, however, the angular accelerations should

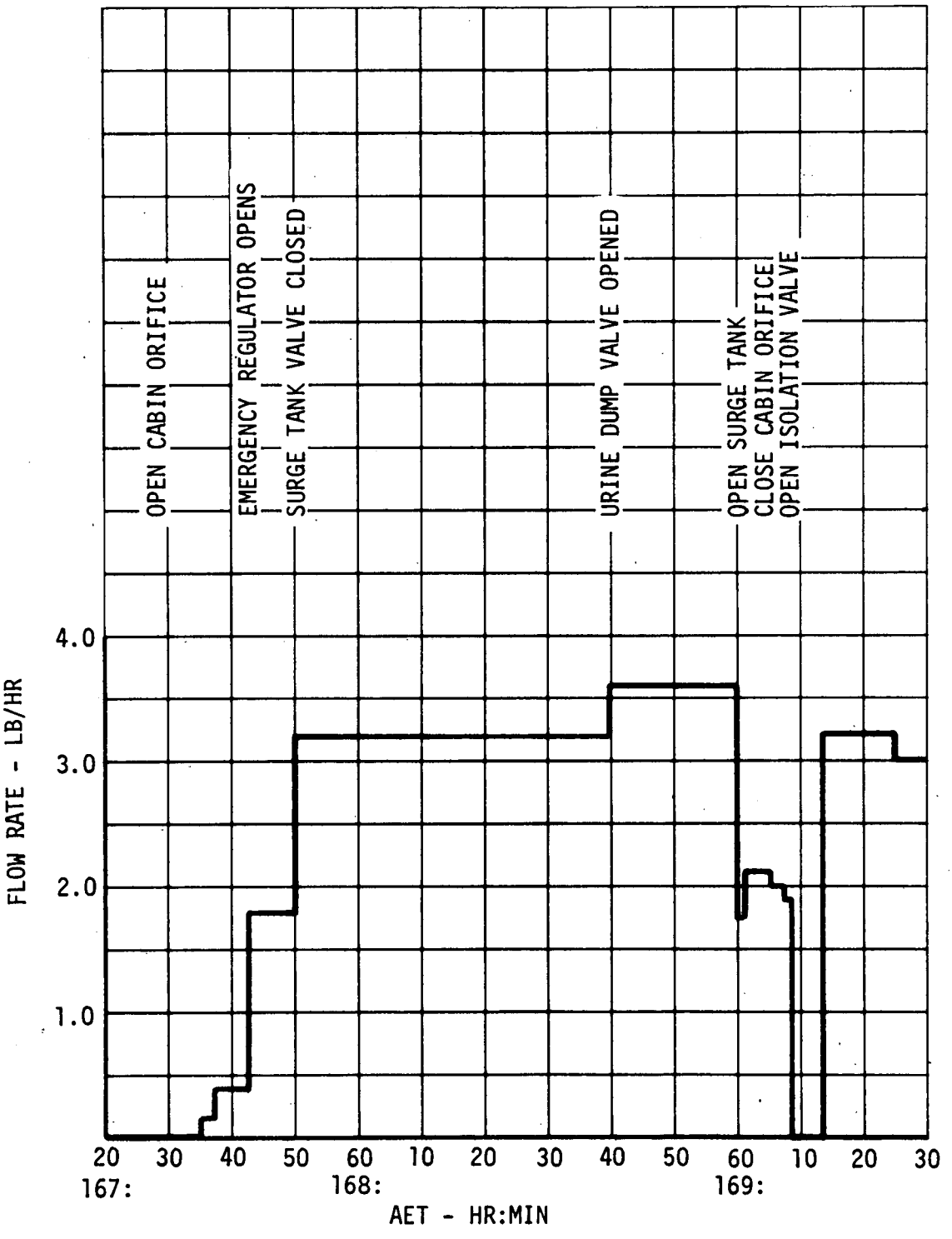

FIGURE 3 - TANK 3 TEST FLOW RATE

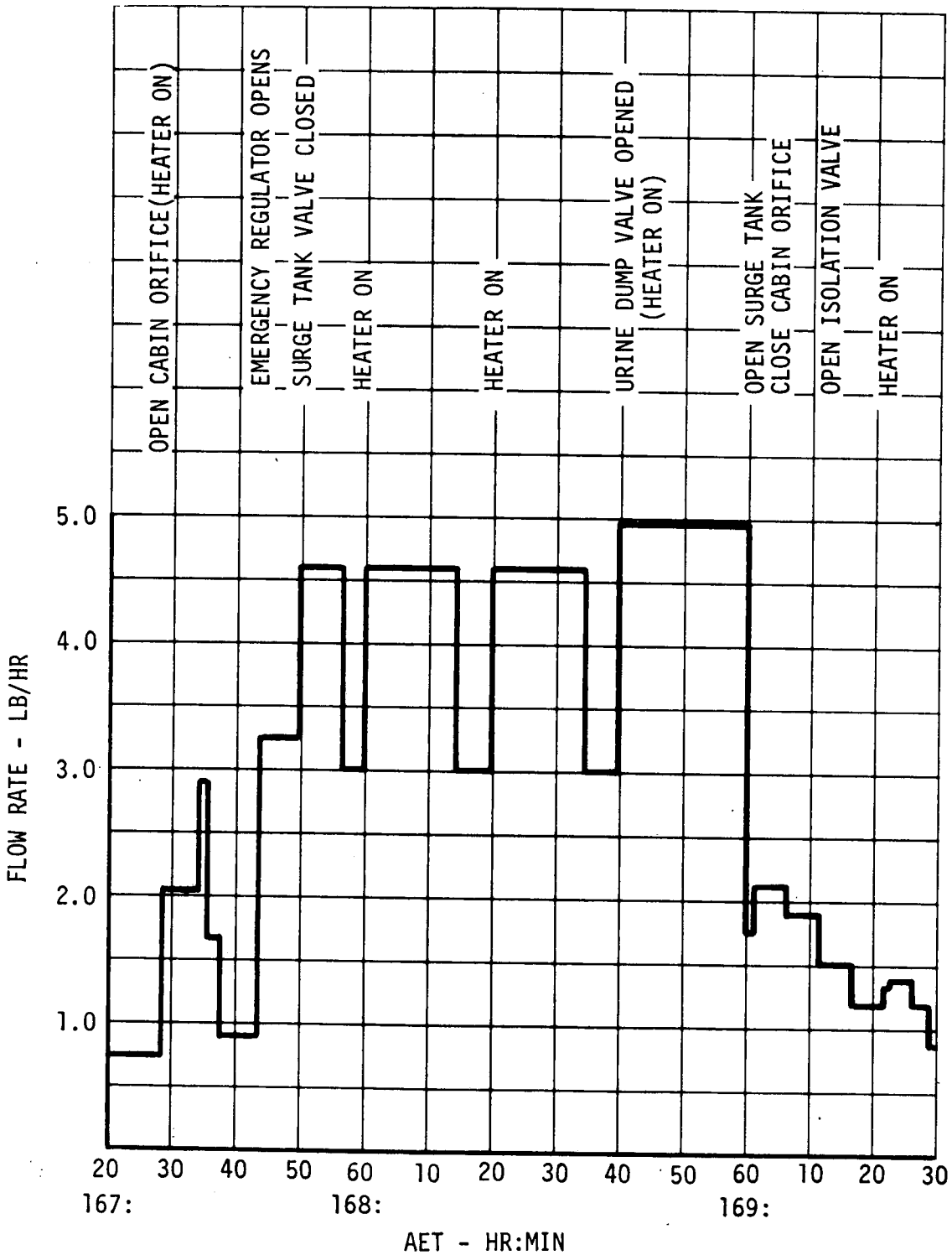

FIGURE 4 - TANK 1 TEST FLOW RATE

certainly not be entirely ignored. The approach used was to distribute the angular acceleration over time intervals of 10 seconds or greater by numerical differentiation of the observed angular rates at the end points of the time interval. The time intervals were selected on the basis of engineering judgement to adequately characterize the acceleration events. Although this procedure is arbitrary, the results appear to be satisfactory and a better method has not presented itself. Tank accelerations during an Apollo 12 attitude hold condition were typically 5×10^{-8} to 7×10^{-8} "g".

The tank accelerations during stable periods of passive thermal control (PTC) were calculated without consideration of angular accelerations. During PTC flight modes, the reaction control system is deactivated and the vehicle is essentially spin stabilized. For this condition, angular accelerations are generally negligible and the centripetal acceleration only is significant.

When the vehicle is in attitude hold in the near vicinity of the earth or moon, the gravity gradient acceleration is significant. This term, which must be added to the rotational accelerations, is:

$$32.174\ \bar{g} = \frac{2\ GM\ (\bar{R}_g \cdot \bar{R}_t)\ \bar{R}_g}{\bar{R}_g^{\,4}\ |\bar{R}_g|} \qquad (4)$$

The gravity gradient term is of the order of 10^{-7} "g" for a 100 mile altitude earth orbit. Since the magnitude of the gravity gradient is proportional to $1/|\bar{R}_g|^3$, the term becomes negligible at distances of 2-3 earth radii. The radius vector to the attracting body in the vehicle coordinate system is necessary to the gravity gradient calculation. This vector can only be determined from the vehicle trajectory and inertial platform data. A computer program for the calculation of the acceleration including the gravity gradient term derived from trajectory data has been developed by NASA-MSC for application to the Apollo 14 mission. The average tank acceleration in lunar orbit was 5×10^{-7} "g" for the Apollo 12 mission.

The tank accelerations for nominal flight conditions can reasonably be assumed to be the same as previous flights at similar conditions. The high flow oxygen tank tests during the Apollo 14 mission were not, however, in nominal flight "g" conditions due to overboard dumping of oxygen. The oxygen dumped overboard through a convergent nozzle in the command module entry hatch produced a significant thrust and vehicle acceleration.

The thrust of the 6.2 lbs/hr oxygen dumped overboard was calculated as the thrust from a choked convergent nozzle for a stagnation temperature of 60°F and a specific heat ratio of 1.4. The resulting

thrust of 0.091 pounds is conservative, since no expansion downstream of the throat or plume effects were considered.

The 0.091 pounds thrust produced a linear "g" of 3.65×10^{-6} for the 24,985 pounds vehicle weight at the time of the test. The thrust vector was not through the vehicle center of mass, therefore, rotational accelerations were also produced. The equation for the angular accelerations is:

$$\bar{R}_f \times \bar{F} = I\,\bar{\alpha} \tag{5}$$

and solving for

$$\bar{\alpha} = I^{-1}\,(\bar{R}_f \times \bar{F}) \tag{6}$$

The moments of inertia obtained from pre-flight mass properties data were used with equation 6 to predict angular acceleration rates. The rotation rates were then calculated from the time required to rotate the vehicle through the 5° dead band. Finally, rotational tank accelerations were calculated from equation 3. The total tank 3 "g" was found to be 4.9×10^{-6} and for tank 1 a "g" of 4.7×10^{-6} was obtained. These accelerations neglected the effects of reaction control system firings as well as plume effects and therefore, may be somewhat lower than actually experienced. The pre-flight acceleration predictions have been used for the high flow test post flight analysis, since acceleration data reduction has not been completed.

ANALYSIS CORRELATIONS WITH FLIGHT DATA

Evaluations of the numerical model and empirical heater temperature equations were based on Apollo 14 flight data. The accelerations and flow rates required by the analyses were determined using the methods described earlier. Comparisons of simulations with Apollo 14 data showed good correlation with the flight pressures and temperatures.

THERMODYNAMIC SIMULATIONS

Detailed tank thermodynamic simulations were conducted with the numerical math model described in the paper* by C. K. Forester. This model uses a rectangular (x and y) grid of cells to approximate the flow fields in the tank. The simulations were accomplished for a range of grid sizes to permit extrapolations of variables to asymptotic limits. The effects of tank elasticity and heater temperature sensor lag were included.

*IBID, page 3.

The tank pressure and heater temperature results from a simulation of one PTC heater cycle are compared with flight data by Figure 5. This simulation was made with a heater area of 0.475 ft^2 which is the flat plate area equivalent to the 0.59 ft^2 outer surface of the cylindrical heater tube. Since the heater tube is perforated, flow through the tube could provide an effective flat plate heater area of 0.95 ft^2. Simulations were conducted for both heater areas to determine which provided the most accurate heater temperature. The results of the convergence analyses for the areas are shown by Figure 6. The asymptotic limit for the heater temperature with the 0.475 ft^2 area is within 9°F of the flight data. The asymptotic temperature with the larger heater area is not in good agreement with flight data. The asymptotic limit of the heater on time for the small heater is also in better agreement with flight data than the large heater. These results imply that the inside of the heater tube is not an effective heat transfer surface.

The simulation of the tank 3 high flow test is shown by Figure 7. The convergence study and the asymptotic limit for the heater temperature are shown by Figure 8. The asymptotic heater temperature with the 0.95 ft^2 heater area is 45°F below flight data. The PTC heater cycle simulation with this area resulted in a heater temperature 95°F below the flight data. Since the 0.475 ft^2 heater area provided good agreement for the PTC heater cycle, the 0.95 ft^2 area was expected to produce temperatures much lower than flight data. The heater temperature simulation results of the PTC heater cycle and the high flow test are contradictory. The contradiction may be due to the "g" level which was estimated as 4.9×10^{-7} "g" for the high flow test. A higher "g" level during the high flow test could bring the results into agreement. The discrepancy could also be due to residual fluid rotations caused by the prior PTC period. Resolution of this discrepancy must await more accurate determination of the "g" level from flight data.

EMPIRICAL HEAT TRANSFER EQUATIONS

Heater temperatures can be determined from the numerical math model, but the computer time requirements are excessive for the generation of parametric data and routine flight analyses. Empirical heat transfer equations were investigated to develop a more convenient tool for heater temperature studies.

The convective heat transfer from a horizontal cylinder is usually determined from a Rayleigh number equation.

$$\frac{dQ}{dt} = \pi \, L \, K \, \Delta T \, C_{ra} \, (R_a)^{1/4} \qquad (7)$$

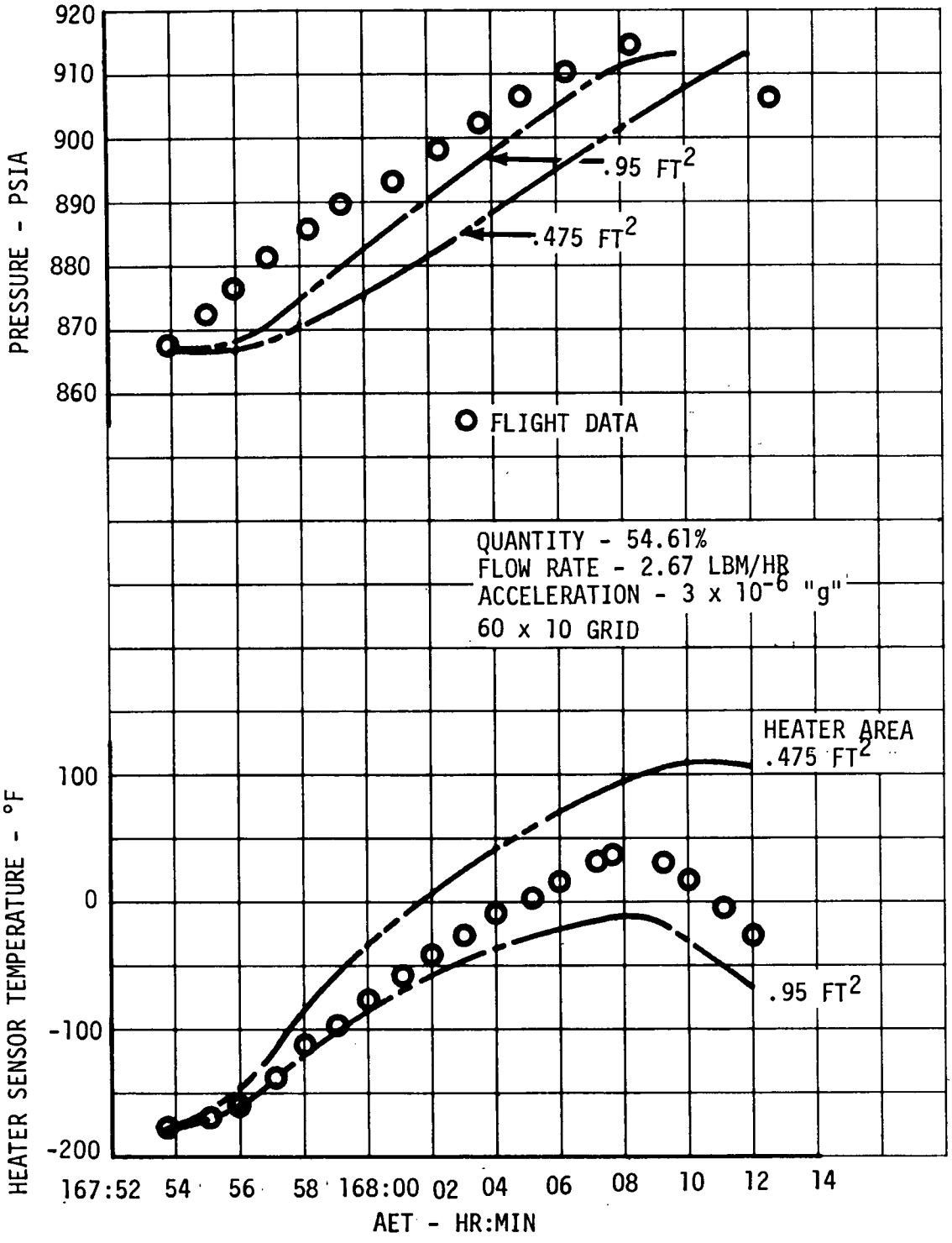

FIGURE 5 - PTC HEATER CYCLE SIMULATION

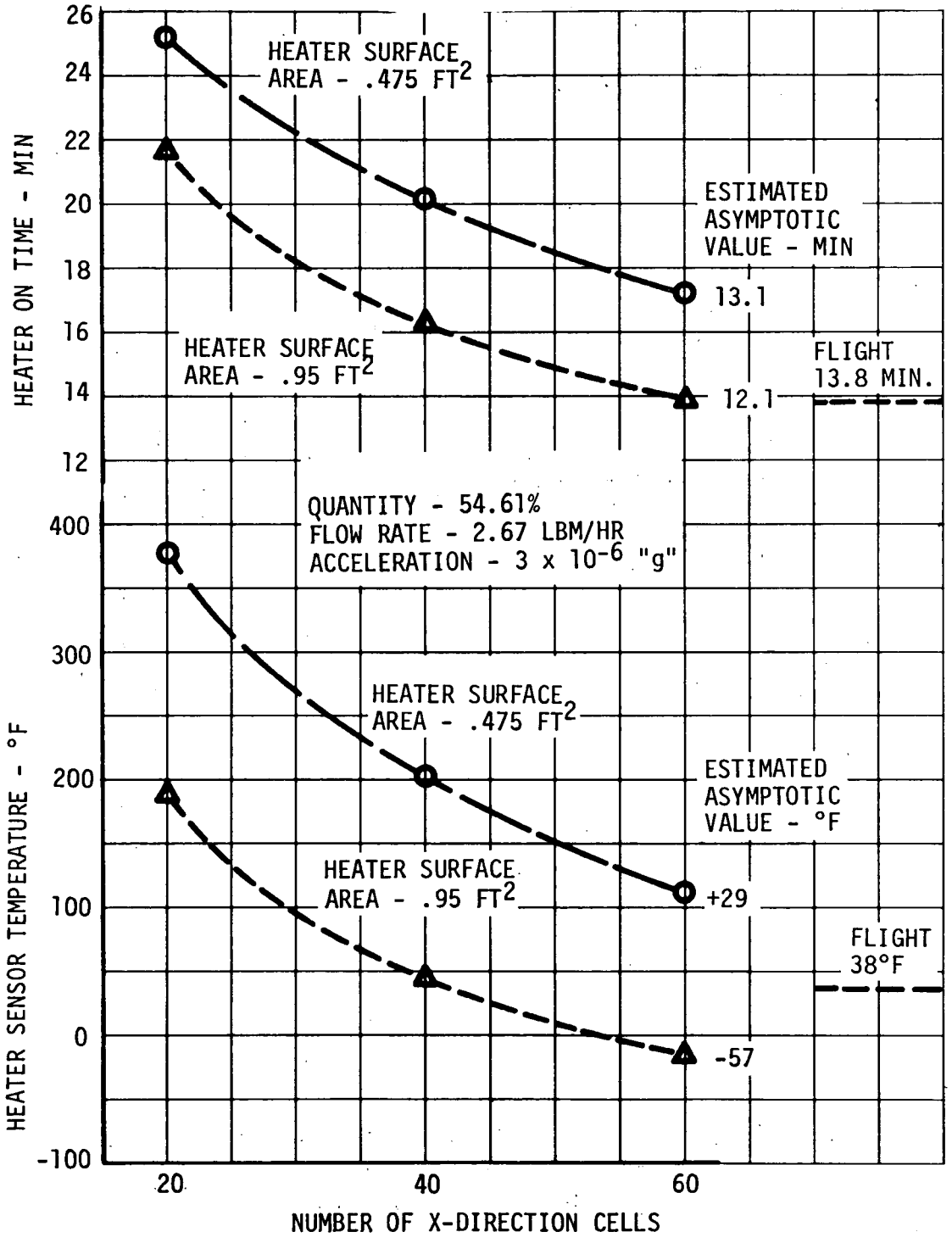

FIGURE 6 - PTC HEATER CYCLE CONVERGENCE

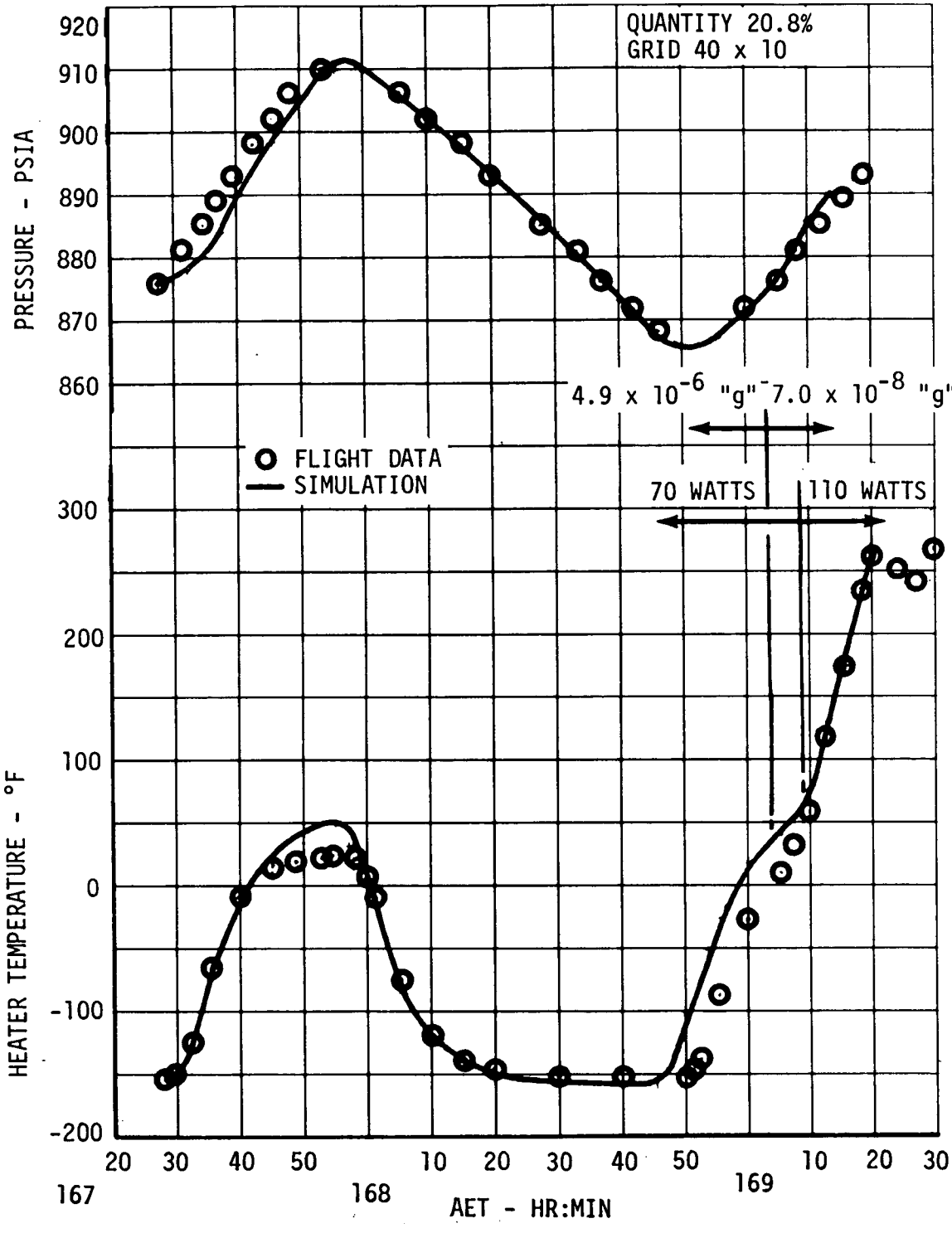

FIGURE 7 - TANK 3 TEST SIMULATION

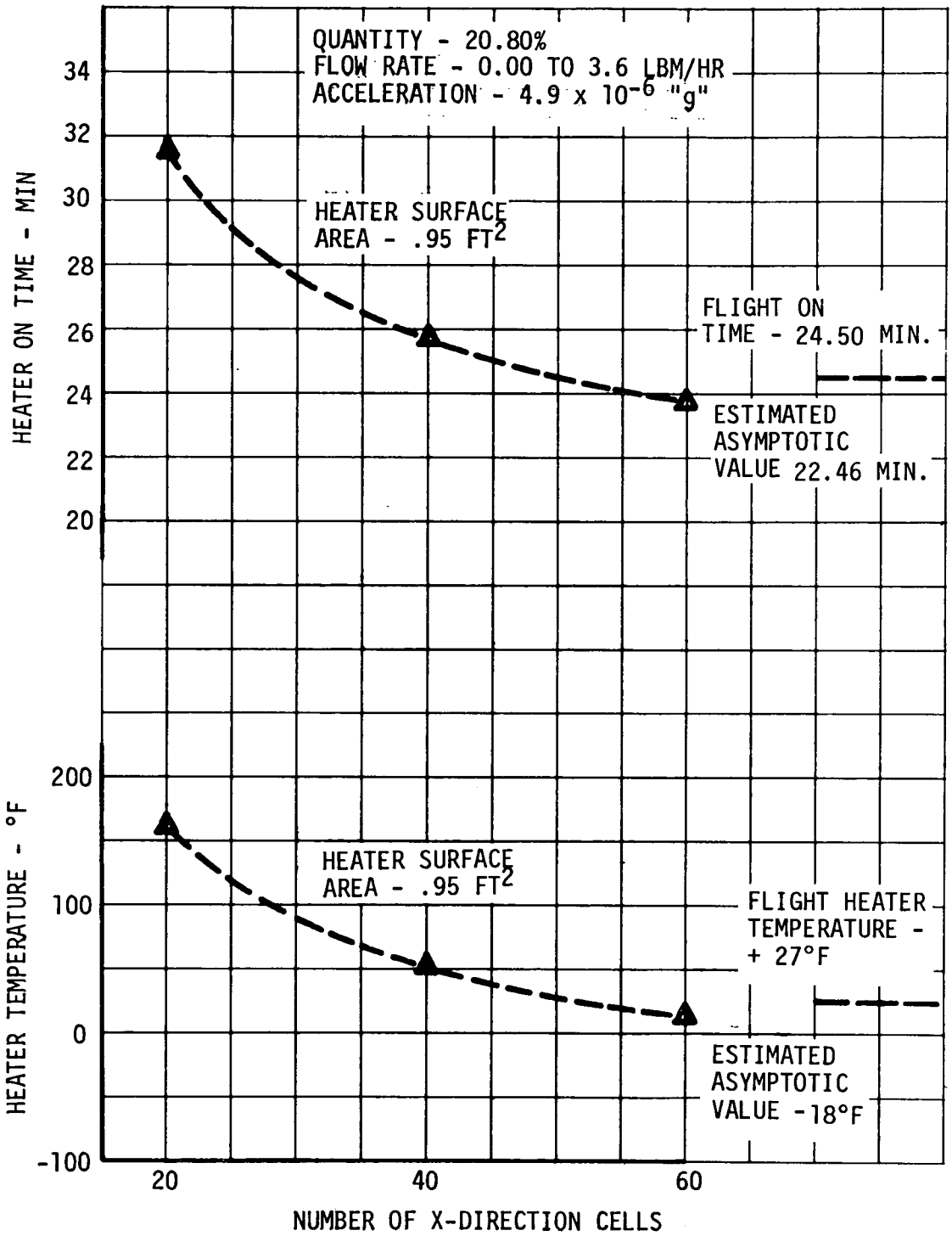

FIGURE 8 - TANK 3 TEST CONVERGENCE

The Rayleigh number is determined from:

$$R_a = \frac{D^3 \rho^2 \, 32.174 \, g \, \beta \, \Delta T \, C_p}{\mu K} \tag{8}$$

The fluid properties used to evaluate the Rayleigh number are usually taken at the mean film temperature. This convention is based on tests with simple fluids under 1 "g" conditions. Since the properties of supercritical oxygen may vary by an order of magnitude in the boundary layer, the properties in the Rayleigh number were averaged instead of taken at the mean film temperature. The viscosity, conductivity, and density were taken as the average of their values for the bulk temperature and the heater temperature. The specific heat was evaluated as the difference in the enthalpy at the heater and bulk temperatures divided by the temperature difference. The coefficient of expansion used was,

$$\beta = \frac{-1}{\rho_b} \frac{\rho_h - \rho_b}{T_h - T_b} \tag{9}$$

The radiation from the heater is also significant and was included in the complete heat transfer equation.

$$\frac{dQ}{dt} = \pi \, L \, K \, \Delta T \, C_{ra} \, (R_a)^{1/4} + \varepsilon \, C_s \, (T_h^4 - T_b^4) \, A \tag{10}$$

Heater temperatures were developed as a function of on time by numerical integration of the equation,

$$\frac{dT}{dt} = \frac{dQ}{dt}\left(\frac{1}{MC}\right) \tag{11}$$

where MC is the heater thermal mass of 0.1 BTU/°F. The heater temperature sensor lag was included in the integration to provide a means of comparison with flight data. The temperature sensor response was determined from:

$$\frac{dT_s}{dt} = C_k \, (T_h - T_s) \tag{12}$$

The temperature-time results of a simulation of one heater cycle using this simplified analysis (Figure 9) are in excellent agreement with flight data. Comparisons between actual and predicted heater temperatures (Figure 10) for several heater cycles indicates predictions within 50°F with the exception of the tank 3 heater cycle during the high flow test. As already mentioned, the "g" level assumed for this period is questionable.

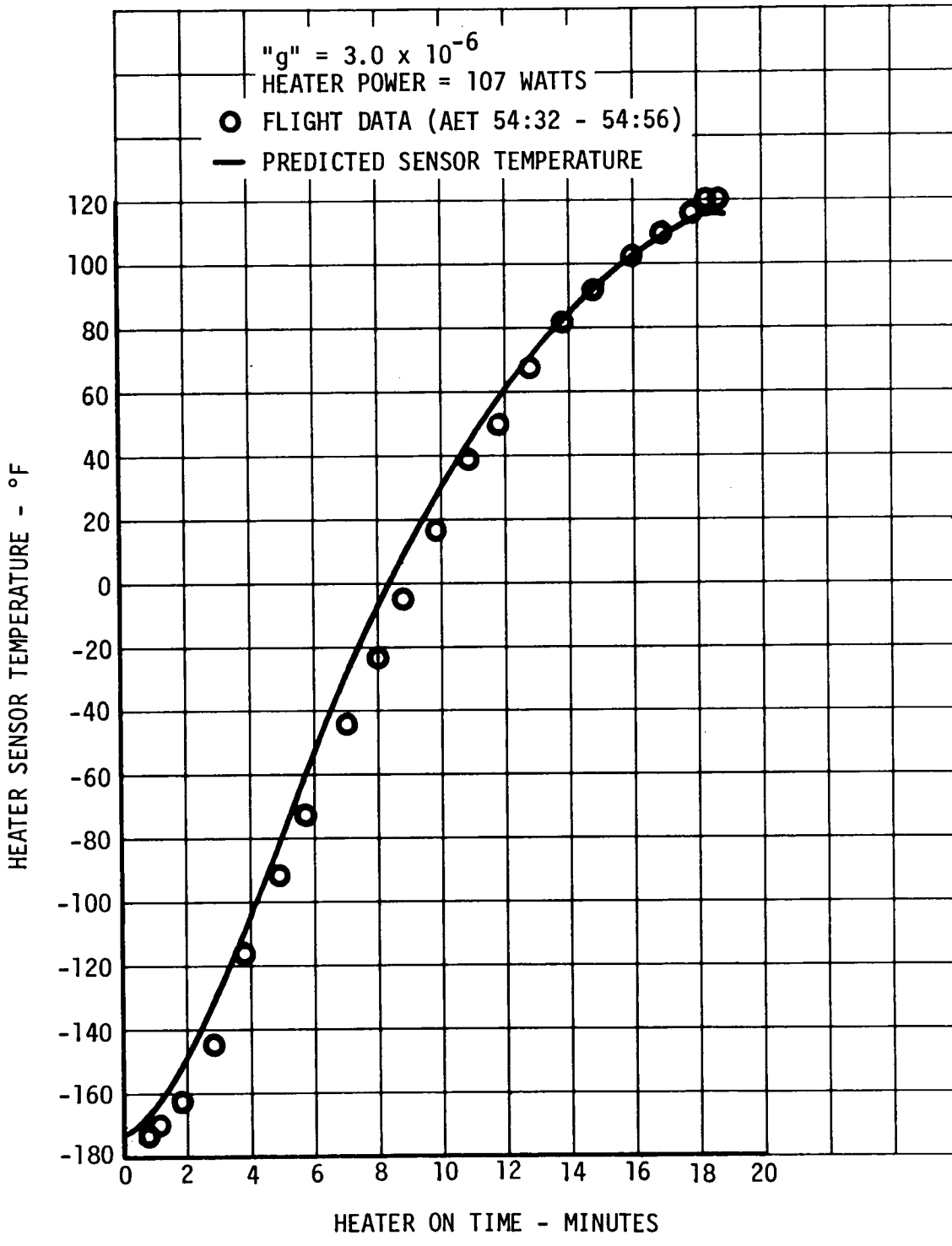

FIGURE 9 - EMPIRICAL HEATER RESPONSE

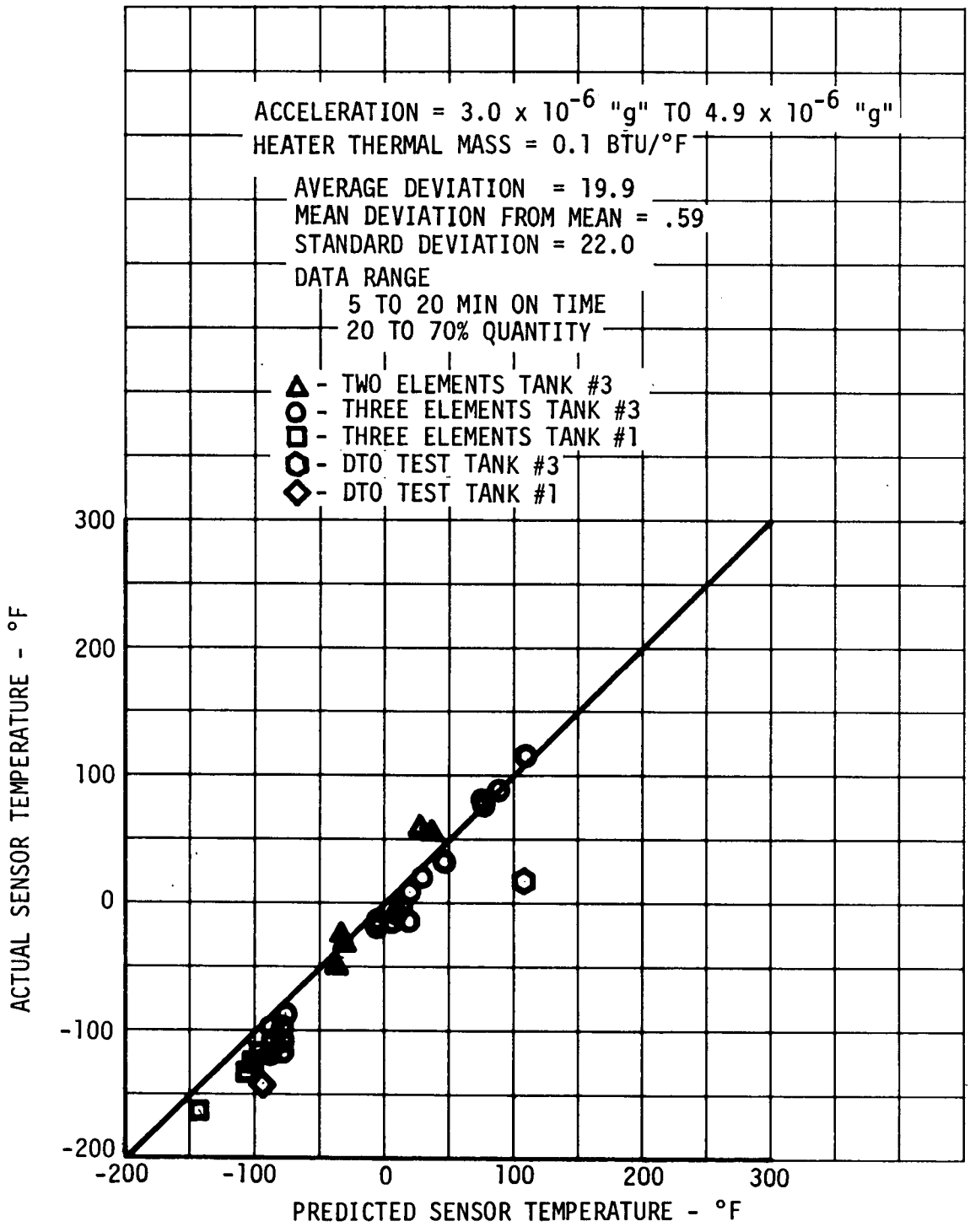

FIGURE 10 - TEMPERATURE COMPARISONS SUMMARY

Parametric heater temperatures (Figure 11) were generated for easy comparisons with flight data. The results of the comparisons made so far are promising, however, the full ranges of quantities and accelerations have not been investigated. A final determination of the empirical constants and the averaging method used for fluid properties can not be made, since attitude hold conditions have not been investigated.

CONCLUSIONS

Conclusions based on correlations with the Apollo 14 high flow tank tests and passive thermal control conditions are:

1. The flight performance of single phase cryogenic tanks can be reasonably predicted using the numerical model developed. Heat transfer and detailed thermodynamic processes (stratification) in the tanks are accurately modeled.

2. Heater temperatures can be predicted from empirical heat transfer equations if fluid properties are averaged instead of evaluated at the mean film temperature.

3. The accuracy of performance predictions is dependent on the ability to predict or control flight accelerations and flow rates.

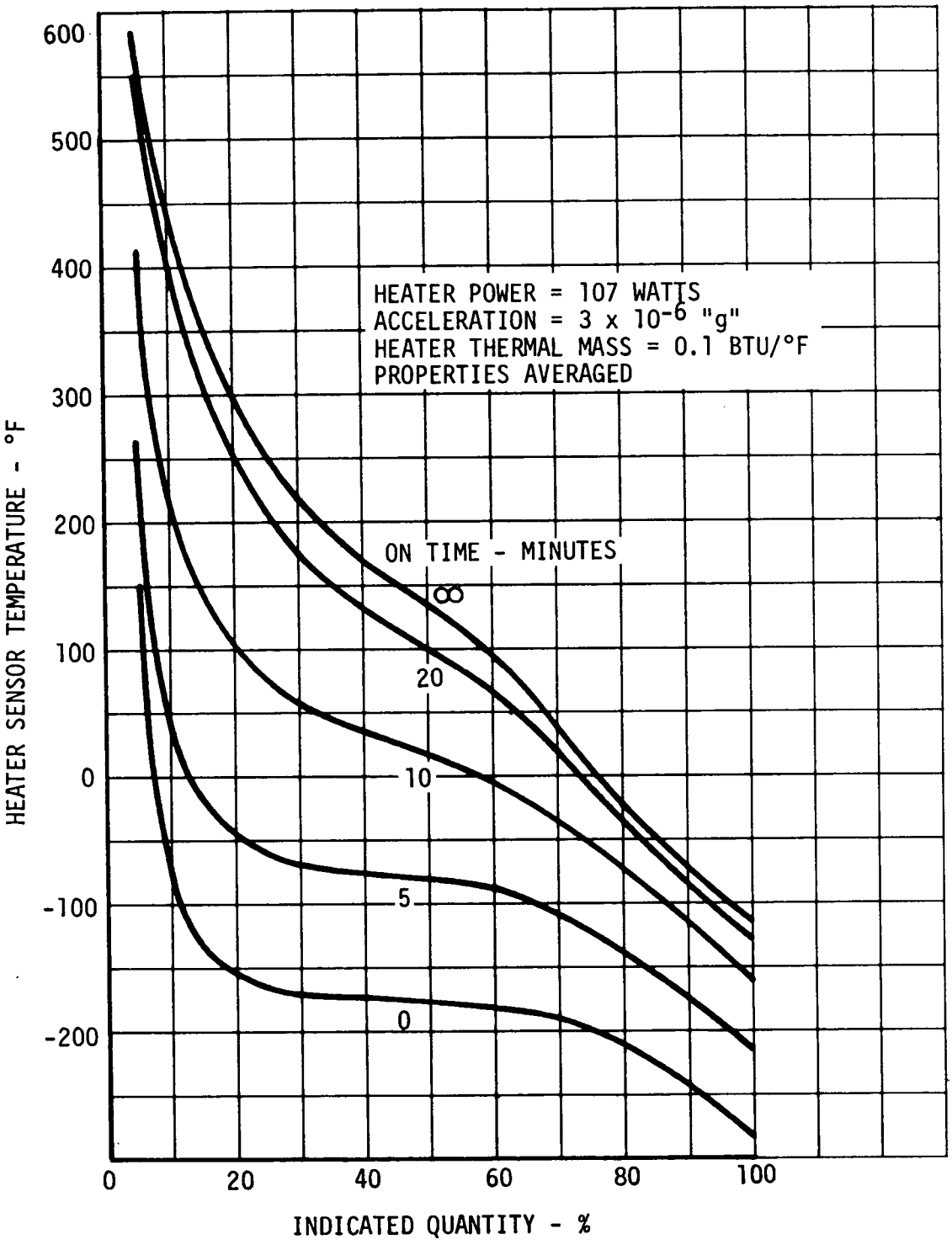

FIGURE 11 - PARAMETRIC HEATER TEMPERATURES

APPENDIX

THE PRESSURE CHANGE EQUATION FOR A CRYOGENIC TANK

The pressure changes in a cryogenic tank resulting from heat addition and mass extraction are usually calculated with the assumption that the tank is a constant volume container. This assumption causes large errors when the fluid is nearly incompressible and the pressure vessel is highly stressed. An error in the pressure change calculation is also caused by flows not usually measured that are required to pressurize plumbing system volumes at ambient temperature. In order to eliminate these errors, the pressure change equation for an equilibrium fluid in an elastic container has been derived and a method for including the external volume effects developed.

The thermodynamic system is bounded by the inside surface of the pressure vessel and is closed at the fluid outlet from the pressure vessel. The volume inside the thermodynamic boundary is not constant since the pressure vessel is elastic. The outflow velocity is assumed to be small enough that the kinetic energy and momentum of the outflow are negligible. The conservation equations for mass and energy, therefore, determine the system response to heat and mass flows.

The conservation of mass:

$$\frac{dM}{dt} = V\frac{d\rho}{dt} + \rho\frac{dV}{dt} \tag{A-1}$$

The conservation of energy:

$$\frac{d}{dt}(\rho VU) = \frac{dQ}{dt} + h\frac{dM}{dt} - P\frac{dV}{dt} \tag{A-2}$$

Expanding A-2 and using the definition of enthalpy

$$\rho V\frac{dU}{dt} + U\left(V\frac{d\rho}{dt} + \rho\frac{dV}{dt}\right) = \frac{dQ}{dt} + \frac{dM}{dt}\left(U + \frac{P}{\rho}\right) - P\frac{dV}{dt} \tag{A-3}$$

Substituting A-1 in A-3 and simplifying

$$\rho V\frac{dU}{dt} = \frac{dQ}{dt} + \frac{P}{\rho}\frac{dM}{dt} - P\frac{dV}{dt} \tag{A-4}$$

The internal energy is taken as a function of pressure and density

$$\frac{dU}{dt} = \frac{\partial U}{\partial P}\frac{dP}{dt} + \frac{\partial U}{\partial \rho}\frac{d\rho}{dt} \tag{A-5}$$

Using A-1 and noting that $M = \rho V$

$$\frac{dU}{dt} = \frac{\partial U}{\partial P}\frac{dP}{dt} + \frac{\partial U}{\partial \rho}\left(\frac{1}{V}\frac{dM}{dt} - \frac{M}{V^2}\frac{dV}{dt}\right) \tag{A-6}$$

Substituting A-6 in A-4

$$\rho V\left[\frac{\partial U}{\partial P}\frac{dP}{dt} + \frac{\partial U}{\partial \rho}\left(\frac{1}{V}\frac{dM}{dt} - \frac{M}{V^2}\frac{dV}{dt}\right)\right] = \frac{dQ}{dt} + \frac{P}{\rho}\frac{dM}{dt} - P\frac{dV}{dt} \tag{A-7}$$

Solving for $\frac{dP}{dt}$ and rearranging

$$\frac{dP}{dt} = \frac{\frac{dQ}{dt} + \frac{P}{\rho}\frac{dM}{dt} - P\frac{dV}{dt} - \rho\frac{\partial U}{\partial \rho}\left(\frac{dM}{dt} - \frac{M}{V}\frac{dV}{dt}\right)}{\rho V\frac{\partial U}{\partial P}} \tag{A-8}$$

Rearranging

$$\frac{dP}{dt} = \frac{\frac{dQ}{dt} + \frac{dM}{dt}\left(\frac{P}{\rho} - \rho\frac{\partial U}{\partial \rho}\right)}{\rho V\frac{\partial U}{\partial P}} + \frac{\rho\frac{\partial U}{\partial \rho}\frac{M}{V}\frac{dV}{dt} - P\frac{dV}{dt}}{\rho V\frac{\partial U}{\partial P}} \tag{A-9}$$

and reducing the last term

$$\frac{dP}{dt} = \frac{\frac{dQ}{dt} + \frac{dM}{dt}\left(\frac{P}{\rho} - \rho\frac{\partial U}{\partial \rho}\right)}{\rho V\frac{\partial U}{\partial P}} + \frac{\rho^2\frac{dV}{dt}\left(\frac{\partial U}{\partial \rho} - \frac{P}{\rho^2}\right)}{\rho V\frac{\partial U}{\partial P}} \tag{A-10}$$

Now define

$$\phi = \frac{1}{\rho\frac{\partial U}{\partial P}} \tag{A-11}$$

and

$$\theta = -\rho\frac{\partial h}{\partial \rho} \equiv -\rho\left(\frac{\partial U}{\partial \rho} - \frac{P}{\rho^2}\right) \tag{A-12}$$

Substituting A-11 and A-12 in A-10

$$\frac{dP}{dt} = \frac{\phi}{V}\left(\frac{dQ}{dt} + \theta\frac{dM}{dt}\right) - \frac{1}{V}\frac{dV}{dt}\rho\theta\phi \qquad \text{(A-13)}$$

Equation A-13 provides a convenient method for calculating pressure response if the volume rate of change is known. The last term is zero for a constant volume system. If the container is elastic so that the volume change is related to the pressure change, some further reduction is possible.

$$\frac{dP}{dt} = \frac{\phi}{V}\left(\frac{dQ}{dt} + \theta\frac{dM}{dt}\right) - \frac{1}{V}\frac{dV}{dP}\frac{dP}{dt}\rho\theta\phi \qquad \text{(A-14)}$$

Again solving for $\frac{dP}{dt}$

$$\frac{dP}{dt} = \frac{\frac{\phi}{V}\left(\frac{dQ}{dt} + \theta\frac{dM}{dt}\right)}{1 + \frac{1}{V}\frac{dV}{dP}\rho\theta\phi} \qquad \text{(A-15)}$$

for a spherical tank

$$\frac{1}{V}\frac{dV}{dP} = \frac{3\ r\ (1-\sigma)}{2\ b\ E} \qquad \text{(A-16)}$$

therefore

$$\frac{dP}{dt} = \frac{\frac{\phi}{V}\left(\frac{dQ}{dt} + \theta\frac{dM}{dt}\right)}{1 + \frac{3\ r\ (1-\sigma)}{2\ b\ E}\rho\theta\phi} \qquad \text{(A-17)}$$

Now the outflow is measured at the end of the distribution lines which contain gas at the same pressure as the tank. The flow across the thermodynamic boundary must include the flow required to pressurize the lines. Two assumptions for determining the flow into the lines may be considered:

1. Fluid expelled from the tanks thermodynamic boundary maintains its density while compressing gas in the lines either adiabatically or isothermally.

2. Fluid expelled from the tank does not affect the temperature distribution from the thermodynamic boundary to the system outlet, but the density in the lines changes adiabatically or isothermally.

The phenomena of assumption 1 can be described by writing the polytropic relationship for the volume of gas in the lines.

$$\frac{V_L}{V_{L_o}} = \left(\frac{P}{P_o}\right)^{-\frac{1}{N}} \tag{A-18}$$

Taking logarithms and differentiating we have:

$$\frac{dV_L}{V_L} = -\frac{1}{N}\frac{dP}{P} \tag{A-19}$$

The flow rate into the tank thermodynamic boundary due to the lines is therefore:

$$\frac{dM_L}{dt} = -\rho_t \frac{V_L}{NP}\frac{dP}{dt} \tag{A-20}$$

Where N=1 for isothermal compression and N=1.4 for adiabatic compression.

Now writing A-14 in terms of the demand and line flow rates.

$$\frac{dP}{dt} = \frac{\phi}{V}\frac{dQ}{dt} + \frac{\phi\theta}{V}\frac{dM_L}{dt} + \frac{\phi\theta}{V}\frac{dM_d}{dt} - \frac{1}{V}\frac{dV}{dP}\frac{dP}{dt}\rho\phi\theta \tag{A-21}$$

Substituting A-20 in A-21 and again solving for $\frac{dP}{dt}$ we have:

$$\frac{dP}{dt} = \frac{\frac{\phi}{V}\left(\frac{dQ}{dt} + \theta\frac{dM_d}{dt}\right)}{1 + \frac{\rho\theta\phi}{V_t}\frac{dV}{dP} + \frac{\rho\theta\phi}{NP}\frac{V_L}{V_t}} \tag{A-22}$$

The relationships for assumption 2 are developed by assuming that the fluid density in the lines is related to the pressure by the polytropic exponent.

$$\rho = \rho_o\left(\frac{P}{P_o}\right)^{\frac{1}{N}} \tag{A-23}$$

Again taking logarithms and differentiating we have:

$$\frac{d\rho}{\rho} = \frac{1}{N}\frac{dP}{P} \tag{A-24}$$

Therefore, the flow rate into the tank from the lines is:

$$\frac{dM_L}{dt} = - \frac{\rho_L Y_L}{NP} \frac{dP}{dt} \qquad \text{(A-25)}$$

Substituting A-25 into A-14 and solving for $\frac{dP}{dt}$ as before we have:

$$\frac{dP}{dt} = \frac{\frac{\phi}{V}\left(\frac{dQ}{dt} + \theta\frac{dM_d}{dt}\right)}{1 + \frac{\rho_t \phi\theta}{V_t}\frac{dV_t}{dP} + \frac{\rho_L \phi\theta}{NP}\frac{V_L}{V_t}} \qquad \text{(A-26)}$$